Measurement of 1323 and 1487 keV resonances in $^{15}N(\alpha,\gamma)^{19}F$ with the recoil separator ERNA

Gianluca Imbriani
Physics Department of University of Naples Federico II,
Italian National Institute of Nuclear Physics (INFN) and
Joint Institute of Nuclear Astrophysics (JINA)

gianluca.imbriani@na.infn.it

Origin of Fluorine: State of the art

^{19}F production site is a longstanding problem, three are the possible **astrophysical sites**:

1. Via spallation of ^{20}Ne by ν_μ and ν_τ neutrinos during the explosion of a **type II Supernovae**;

2. In massive stars experiencing large mass loss episodes, where the material exposed to the He burning could be ejected before the fluorine destruction occurring via the **$^{19}F(\alpha,p)^{22}Ne$** reaction (**Wolf Rayet stars**);

3. During the **Asymptotic Giant Branch (AGB)**, where the ^{19}F production takes place, mainly via the **$^{15}N(\alpha,\gamma)^{19}F$** reaction, in the convective zones generated by recursive He-burning thermonuclear runaways. **Most promising**

Observation of the ^{19}F

- Direct information of ^{19}F production only in AGB stars .

ABIA ET AL. THE ASTROPHYSICAL JOURNAL LETTERS, 737:L8 (5pp), 2011 August 10

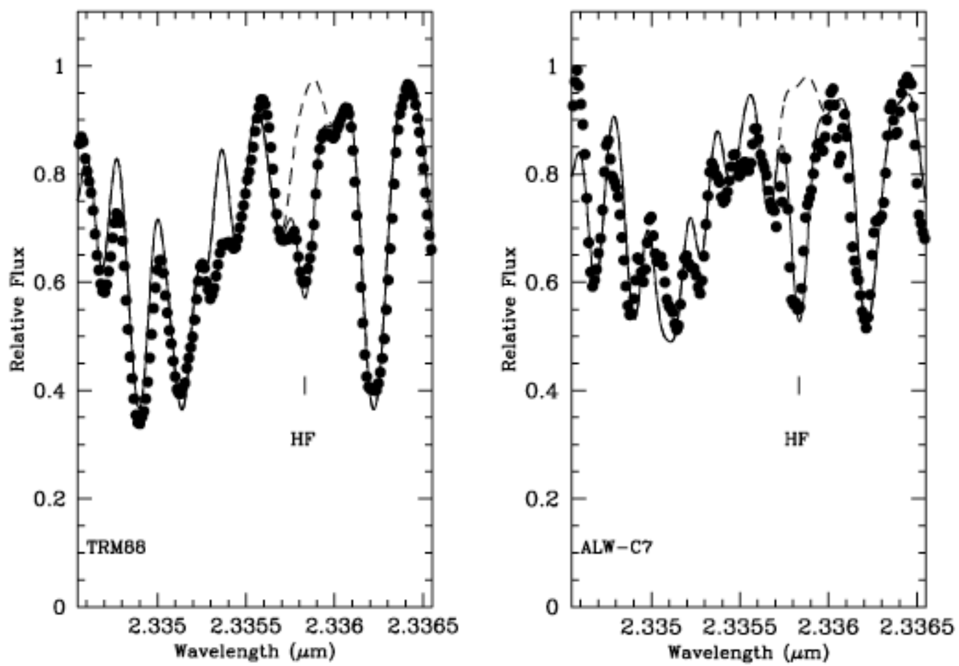

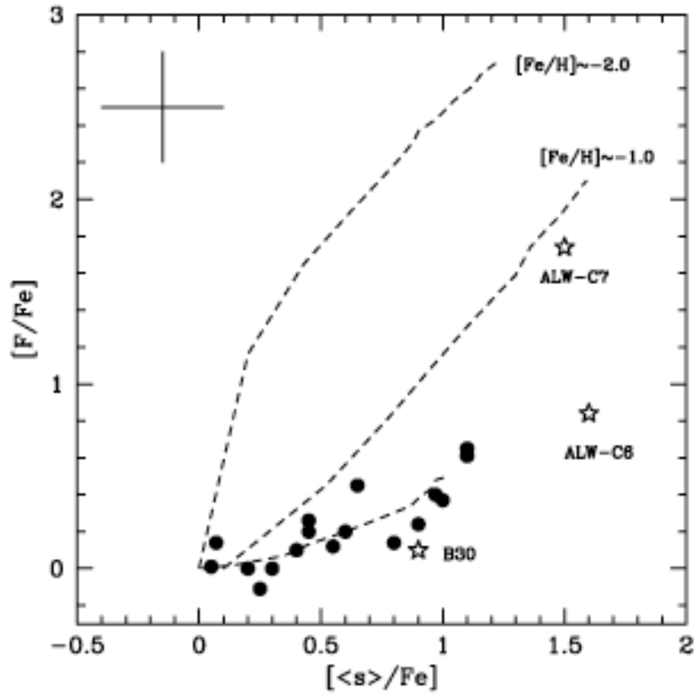

^{19}F Observation is still not very well understood, but is not as large as considered before

^{19}F production during the AGB phase 1st

To produce **^{19}F** it is necessary to accumulate **^{15}N** in the **He–intershell**, where the reaction **^{15}N(α,γ)^{19}F** takes place.
This can happen during the AGB phase, when alternatively H and He-shells switch on and off several times. Then, the convective **H-envelope** can penetrate the **He-intershell**, dredging-up the fluorine.

Asymptotic Giant Branch

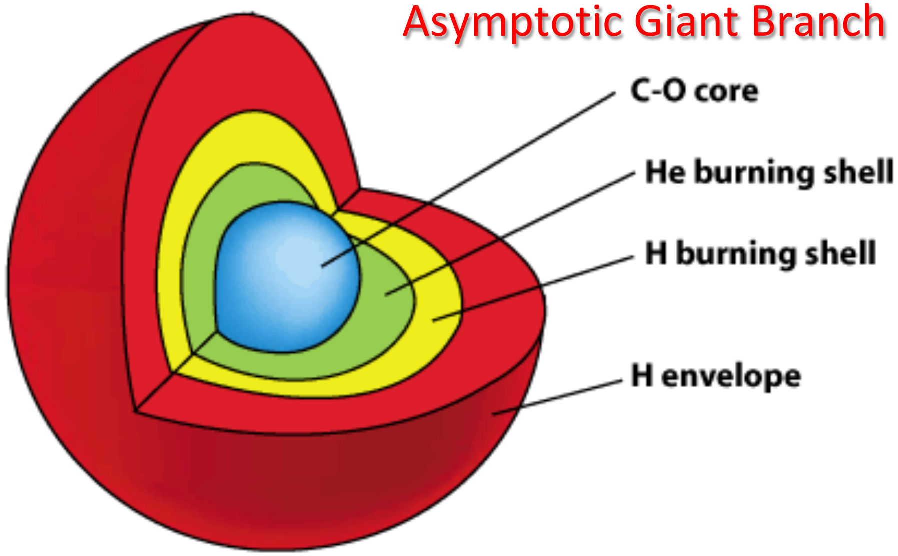

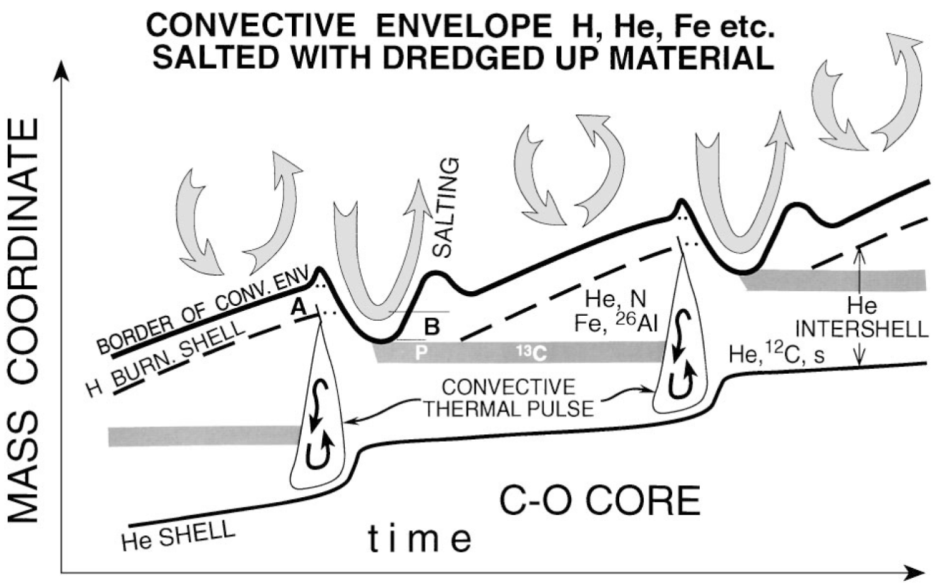

Nuclear network:

1. Accumulation of ^{15}N:

A. ^{13}C(α,n)^{16}O $\rightarrow$ ^{14}N(n,p)^{14}C

B. ^{14}C(α,γ)^{18}O, ^{14}N(α,γ)^{18}F(β^+)^{18}O

C. ^{18}O(p,α)^{15}N, the presence of p could destroy ^{5}N via ^{15}N(p,α)^{12}C.

2. When temperature increases:

A. ^{15}N(α,γ)^{19}F

To start the nuclear network, which will end with the ^{19}F, it is thus required the concomitant presence of neutrons and protons.

^{19}F production during the AGB phase 2nd

Summing up, the final ^{19}F abundance strongly depends on the reactions governing the ^{15}N and the ^{18}O nucleosynthesis.
The complete list of reactions that is worth to explore is:

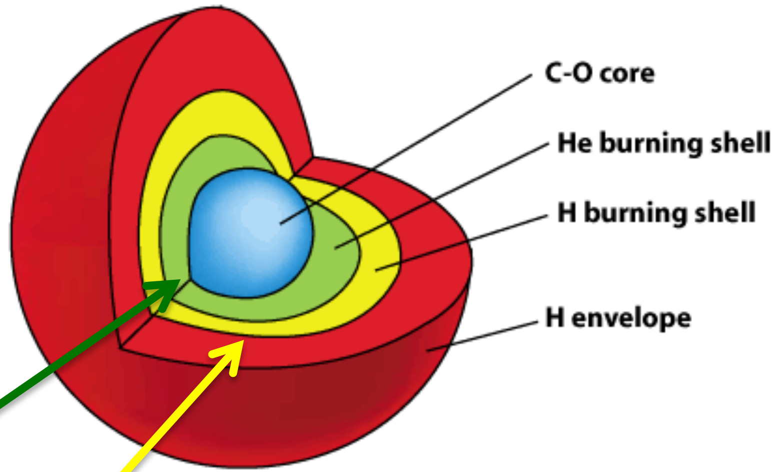

$^{13}C(\alpha,n)^{16}O$, $^{14}C(\alpha,\gamma)^{18}O$, $^{14}N(\alpha,\gamma)^{18}F$, $^{15}N(\alpha,\gamma)^{19}F$, $^{18}O(\alpha,\gamma)^{22}Ne$, $^{18}F(\alpha,p)^{21}Ne$ and $^{19}F(\alpha,p)^{22}Ne$.

$^{15}N(p,\gamma)^{16}O$, $^{17}O(p,\gamma)^{18}F(\beta^+)^{18}O$, $^{18}O(p,\gamma)^{19}F$, $^{15}N(p,\alpha)^{12}C$, $^{18}O(p,\alpha)^{15}N$,

The temperature in the H shell of AGB star is between $20\cdot10^6$ K and $80\cdot10^6$ K, while in the He shell ranges between $100\cdot10^6$ K and $400\cdot10^6$ K.

Stellar models with FUNS*

Updating the nuclear network rates

S. Cristallo et al.: ^{19}F nucleosynthesis at low metallicities *(RN)* A&A 570, A46 (2014)

Reaction rate	Old source	New source
1 Proton captures		
$^{14}N(p,\gamma)^{15}O$	Formicola et al. (2004)	Adelberger et al. (2011)
$^{15}N(p,\gamma)^{16}O$	Angulo et al. (1999)	Leblanc et al. (2010)
$^{17}O(p,\gamma)^{18}F$	Angulo et al. (1999)	Scott et al. (2012)
$^{18}O(p,\gamma)^{19}F$	Angulo et al. (1999)	Iliadis et al. (2010)
$^{15}N(p,\alpha)^{12}C$	Angulo et al. (1999)	Angulo et al. (1999)
$^{17}O(p,\alpha)^{14}N$	Angulo et al. (1999)	Iliadis et al. (2010)
$^{18}O(p,\alpha)^{15}N$	Angulo et al. (1999)	Iliadis et al. (2010)
$^{19}F(p,\alpha)^{16}O$	Angulo et al. (1999)	La Cognata et al. (2011)
α captures		
$^{14}C(\alpha,\gamma)^{18}O$	Caughlan & Fowler (1988)	Lugaro et al. (2004)
$^{14}N(\alpha,\gamma)^{18}F$	Görres et al. (2000)	Iliadis et al. (2010)
$^{15}N(\alpha,\gamma)^{19}F$	Angulo et al. (1999)	Iliadis et al. (2010)
$^{18}O(\alpha,\gamma)^{22}Ne$	Giesen et al. (1994)	Iliadis et al. (2010)
$^{19}F(\alpha,p)^{22}Ne$	Ugalde (2005)	Ugalde et al. (2008)
$^{13}C(\alpha,n)^{16}O$	Drotleff et al. (1993)	Heil et al. (2008)

* Cristallo, S., Straniero, O., Gallino, R., et al. 2009, ApJ, 696, 797
Straniero, O., Gallino, R., & Cristallo, S. 2006, Nucl. Phys. A, 777, 311

Sensitivity study

Table 2. 2σ percentage cross section upper and lower uncertainties at $T = 1 \times 10^8$ K and $T = 2.5 \times 10^8$ K and corresponding percentage fluorine surface variations.

Reaction rate	2σ ($T_8 = 1$) Upper	2σ ($T_8 = 1$) Lower	2σ ($T_8 = 2.5$) Upper	2σ ($T_8 = 2.5$) Lower	Δ [F/Fe] (% var.) Upper	Δ [F/Fe] (% var.) Lower	Δ [F/$\langle$s$\rangle$] (% var.) Upper	Δ [F/$\langle$s$\rangle$] (% var.) Lower
$^{14}N(p,\gamma)^{15}O$	10	10	8	8	–3	+5	–3	+3
$^{15}N(p,\gamma)^{16}O$	15	15	15	15	–1	–2	–3	–2
$^{17}O(p,\gamma)^{18}F$	15	15	20	20	0	–2	–3	0
$^{18}O(p,\gamma)^{19}F$	30	30	30	30	–2	–3	–1	–3
$^{15}N(p,\alpha)^{12}C$	20	20	15	15	–3	+1	–3	–3
$^{17}O(p,\alpha)^{14}C$	15	15	6	6	–2	–2	–1	0
$^{18}O(p,\alpha)^{15}N$	8	8	8	8	+1	–2	+3	–1
$^{19}F(p,\alpha)^{16}O$	35	35	35	35	0	–1	–4	–4
$^{14}C(\alpha,\gamma)^{18}O$	100	84	100	62	–2	0	–3	–2
$^{14}N(\alpha,\gamma)^{18}F$	20	20	10	10	–1	–1	+3	–1
$^{15}N(\alpha,\gamma)^{19}F$	100	50	15	15	–3	–2	0	+5
$^{18}O(\alpha,\gamma)^{22}Ne$	70	50	70	50	–3	+1	–4	–5
$^{19}F(\alpha,p)^{22}Ne$	100	100	50	50	–5	+2	–2	+4
$^{13}C(\alpha,n)^{16}O$	25	25	25	25	–3	+7	–1	+3

S. Cristallo et al.: ^{19}F nucleosynthesis at low metallicities *(RN)* A&A 570, A46 (2014)

Only $^{14}N(p,\gamma)^{15}O$ and $^{13}C(\alpha,n)^{16}O$ uncertainties influences the F production

Beyond the present uncertainties

Presence of not well know low or sub-threshold energy states in $^{13}C(\alpha,n)^{16}O$, $^{14}C(\alpha,\gamma)^{18}O$, $^{14}N(\alpha,\gamma)^{18}F$, $^{15}N(\alpha,\gamma)^{19}F$, $^{18}O(\alpha,\gamma)^{22}Ne$ and $^{19}F(\alpha,p)^{22}Ne$ may justify a larger variation of the rate

Table 3. Scaling factors sf of the computed tests with the corresponding ^{19}F and $F/\langle s\rangle$ surface ratios with respect to the reference case.

Reaction rate	sf	$R(^{19}F)$	$R(F/\langle s\rangle)$
$^{13}C(\alpha,n)^{16}O$	0.01	4.70	2.80
$^{13}C(\alpha,n)^{16}O$	100	0.62	0.67
$^{14}C(\alpha,\gamma)^{18}O$	0.01	1.03	1.59
$^{14}C(\alpha,\gamma)^{18}O$	100	1.04	1.61
$^{14}N(\alpha,\gamma)^{18}F$	0.01	3.03	5.14
$^{14}N(\alpha,\gamma)^{18}F$	100	0.64	1.10
$^{15}N(\alpha,\gamma)^{19}F$	0.01	0.11	0.12
$^{15}N(\alpha,\gamma)^{19}F$	100	0.96	1.50
$^{18}O(\alpha,\gamma)^{22}Ne$	0.01	2.21	2.01
$^{18}O(\alpha,\gamma)^{22}Ne$	100	0.52	0.52
$^{19}F(\alpha,p)^{22}Ne$	0.01	1.05	1.19
$^{19}F(\alpha,p)^{22}Ne$	100	0.08	0.14

S. Cristallo et al.: ^{19}F nucleosynthesis at low metallicities *(RN)* A&A 570, A46 (2014)

Beyond the present uncertainties

Presence of not well know low or sub-threshold energy states in $^{13}C(\alpha,n)^{16}O$, $^{14}C(\alpha,\gamma)^{18}O$, $^{14}N(\alpha,\gamma)^{18}F$, $^{15}N(\alpha,\gamma)^{19}F$, $^{18}O(\alpha,\gamma)^{22}Ne$ and $^{19}F(\alpha,p)^{22}Ne$ may justify a larger variation of the rate

Table 3. Scaling factors sf of the computed tests with the corresponding ^{19}F and F/⟨s⟩ surface ratios with respect to the reference case.

Reaction rate	sf	$R(^{19}F)$	$R(F/\langle s\rangle)$
$^{13}C(\alpha,n)^{16}O$	0.01	4.70	2.80
$^{13}C(\alpha,n)^{16}O$	100	0.62	0.67
$^{14}C(\alpha,\gamma)^{18}O$	0.01	1.03	1.59
$^{14}C(\alpha,\gamma)^{18}O$	100	1.04	1.61
$^{14}N(\alpha,\gamma)^{18}F$	0.01	3.03	5.14
$^{14}N(\alpha,\gamma)^{18}F$	100	0.64	1.10
$^{15}N(\alpha,\gamma)^{19}F$	0.01	0.11	0.12
$^{15}N(\alpha,\gamma)^{19}F$	100	0.96	1.50
$^{18}O(\alpha,\gamma)^{22}Ne$	0.01	2.21	2.01
$^{18}O(\alpha,\gamma)^{22}Ne$	100	0.52	0.52
$^{19}F(\alpha,p)^{22}Ne$	0.01	1.05	1.19
$^{19}F(\alpha,p)^{22}Ne$	100	0.08	0.14

$^{14}C(a,g)^{18}O$
$^{18}O(a,g)^{22}Ne$
No variation

$^{14}N(a,g)^{18}F$
$^{13}C(a,n)^{16}O$
Small variation

$^{15}N(a,g)^{19}F$
$^{19}F(a,p)^{22}Ne$
Large variation

S. Cristallo et al.: ^{19}F nucleosynthesis at low metallicities (RN) A&A 570, A46 (2014)

Beyond the present uncertainties

Presence of not well know low or sub-threshold energy states in $^{13}C(\alpha,n)^{16}O$, $^{14}C(\alpha,\gamma)^{18}O$, $^{14}N(\alpha,\gamma)^{18}F$, $^{15}N(\alpha,\gamma)^{19}F$, $^{18}O(\alpha,\gamma)^{22}Ne$ and $^{19}F(\alpha,p)^{22}Ne$ may justify a larger variation of the rate

Table 3. Scaling factors sf of the computed tests with the corresponding ^{19}F and $F/\langle s\rangle$ surface ratios with respect to the reference case.

Reaction rate	sf	$R(^{19}F)$	$R(F/\langle s\rangle)$
$^{13}C(\alpha,n)^{16}O$	0.01	4.70	2.80
$^{13}C(\alpha,n)^{16}O$	100	0.62	0.67
$^{14}C(\alpha,\gamma)^{18}O$	0.01	1.03	1.59
$^{14}C(\alpha,\gamma)^{18}O$	100	1.04	1.61
$^{14}N(\alpha,\gamma)^{18}F$	0.01	3.03	5.14
$^{14}N(\alpha,\gamma)^{18}F$	100	0.64	1.10
$^{15}N(\alpha,\gamma)^{19}F$	0.01	0.11	0.12
$^{15}N(\alpha,\gamma)^{19}F$	100	0.96	1.50
$^{18}O(\alpha,\gamma)^{22}Ne$	0.01	2.21	2.01
$^{18}O(\alpha,\gamma)^{22}Ne$	100	0.52	0.52
$^{19}F(\alpha,p)^{22}Ne$	0.01	1.05	1.19
$^{19}F(\alpha,p)^{22}Ne$	100	0.08	0.14

$^{14}C(a,g)^{18}O$
$^{18}O(a,g)^{22}Ne$ → **No variation**

$^{14}N(a,g)^{18}F$
$^{13}C(a,n)^{16}O$ → **Small variation**

$^{15}N(a,g)^{19}F$
$^{19}F(a,p)^{22}Ne$ → **Large variation**

S. Cristallo et al.: ^{19}F nucleosynthesis at low metallicities (*RN*) A&A 570, A46 (2014)

$^{15}N(\alpha,\gamma)^{19}F$

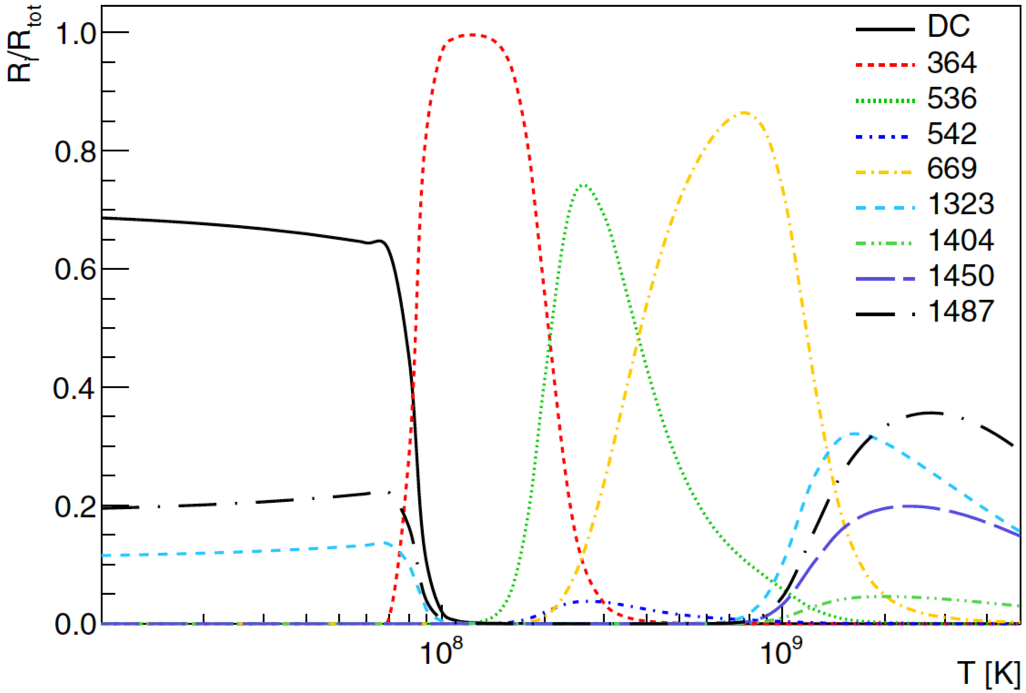

FIG. 11. Fractional contribution of resonances and DC component to the total reaction rate of the $^{15}N(\alpha,\gamma)^{19}F$, as a function of the temperature. The resonances are identified with their center-of-mass energy in keV.

$^{15}N(\alpha,\gamma)^{19}F$

Q-value 4014 keV

E_{cm} [keV]	363.9	536.1	542.3	668	1091.2	1323	1487
$\omega\gamma$ [keV]	$6.0\ 10^{-12}$ u.l	$(9.5 \pm 1.2)\ 10^{-8}$	$(6.4 \pm 2.5)\ 10^{-9}$	$(5.6 \pm 0.6)\ 10^{-6}$	$(9.7 \pm 1.6)\ 10^{-6}$	$(1.69 \pm 0.14)\ 10^{-3}$	$(3.56 \pm 0.28)\ 10^{-3}$
Recoils/day/ μA	1	$8.5\ 10^{3}$	$5.5\ 10^{2}$	$3.8\ 10^{5}$	$3.9\ 10^{5}$	$6\ 10^{8}$	$1\ 10^{9}$

The measurement at ERNA

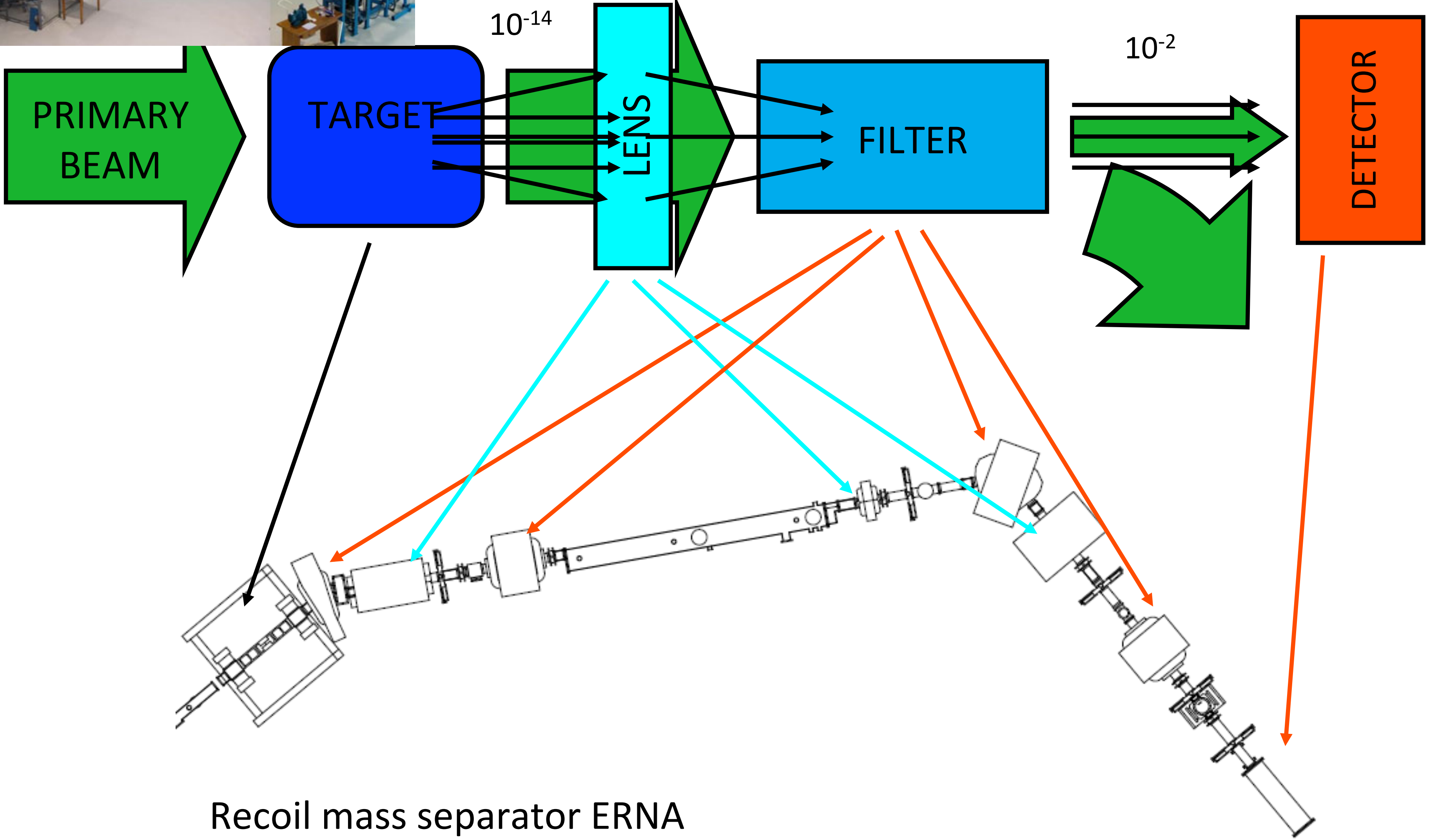

Recoil mass separator ERNA

The measurement at ERNA

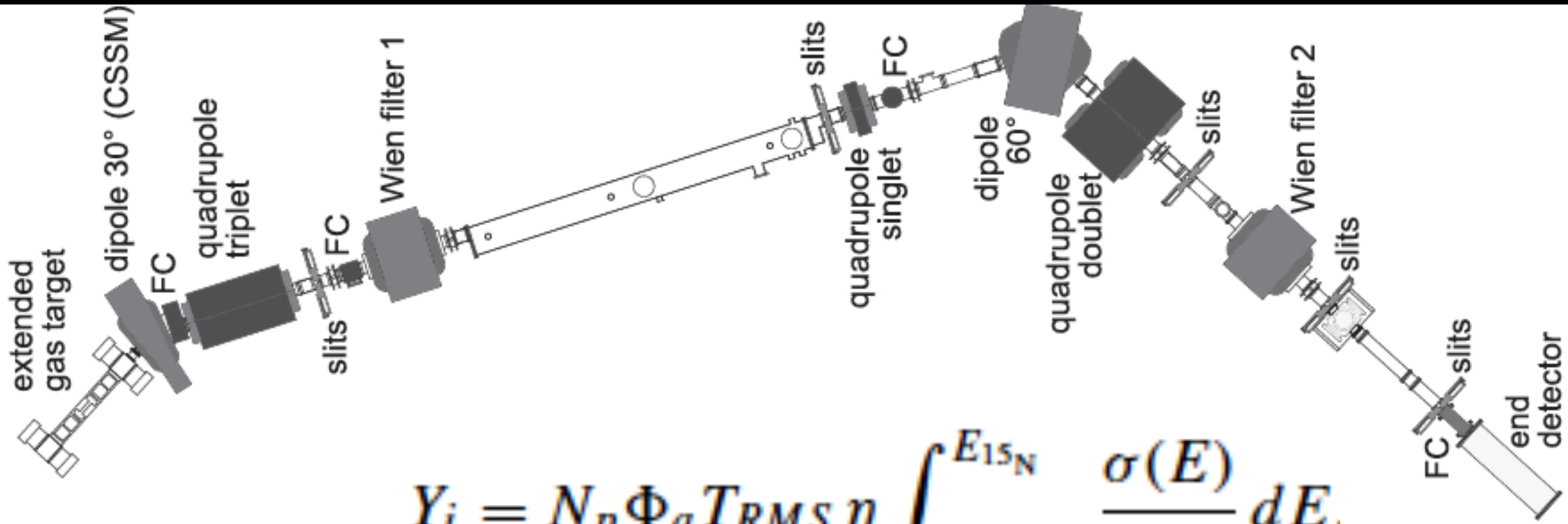

$$Y_i = N_p \Phi_q T_{RMS}\, \eta \int_{E_{^{15}N}-T_t}^{E_{^{15}N}} \frac{\sigma(E)}{\varepsilon(E)}\, dE,$$

- Y_i reaction yields
- N_p is the number of ^{15}N impinging on the target, we monitored this flux using Si Detector at about 25° placed in the second downstream pumping stage;
- Φ_q is the probability of recoils in the q+ charge state entering the separator;
- T_{RMS} is the separator transmission of recoils in charge state q+ to the end detector;
- η is is the detection efficiency;
- T_t is the target thickness.

The N beam

Nitrogen ion beam generation with a source of negative ions by cesium sputtering (**SNICS**) suffers difficulties connected with its low electron negativity, which hampers the formation of a stable negative ion.

material	Mass injected	I_{FC02} [μA]	I_{FC04} [pμA]
BN + C + Ag	26	7.7	2.1 ± 0.5
BN + C + Ag	25	2.5	0.7
$Fe_3K(CN)_6$	26	14.0	4.0 ± 0.5
KSCN	26	11.0	3.5 ± 0.6
$KSC^{15}N$	27	10.0	3.2
Polypyrrole	26	6.0	1.3
NaN_3 + C	26	10.0	2.8
Eumelanin	26	7.0	1.7
Nitroaniline	26	0.3	
BN	25	2.7	0.8
$NaNO_3$	30	0.4	
NH_4NO_3	30	0.03	

Measured N beam current in FC4 as a function of the injected ion mass.

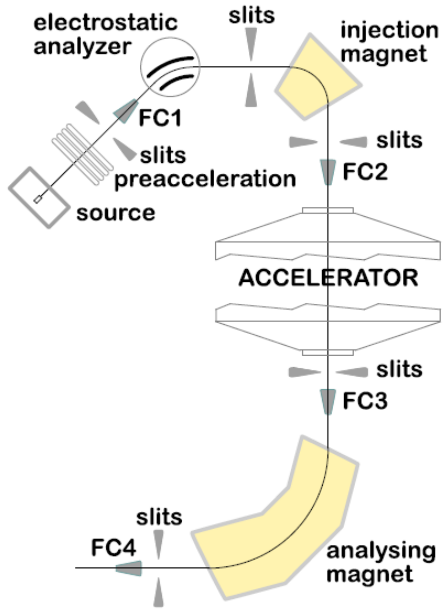

Nuclear Instruments and Methods in Physics Research A 689 (2012) 98–101

Contents lists available at SciVerse ScienceDirect

Nuclear Instruments and Methods in Physics Research A

journal homepage: www.elsevier.com/locate/nima

^{14,15}N beam from cyanide compounds

A. Di Leva [a,b], A. Pezzella [c,b,*], N. De Cesare [d,b], A. D'Onofrio [e,b], L. Gialanella [e,b], M. Romano [a,b], M. Romoli [b], D. Schuermann [a,b], F. Terrasi [e,b], G. Imbriani [a,b,**]

Helium Gas Target thickness

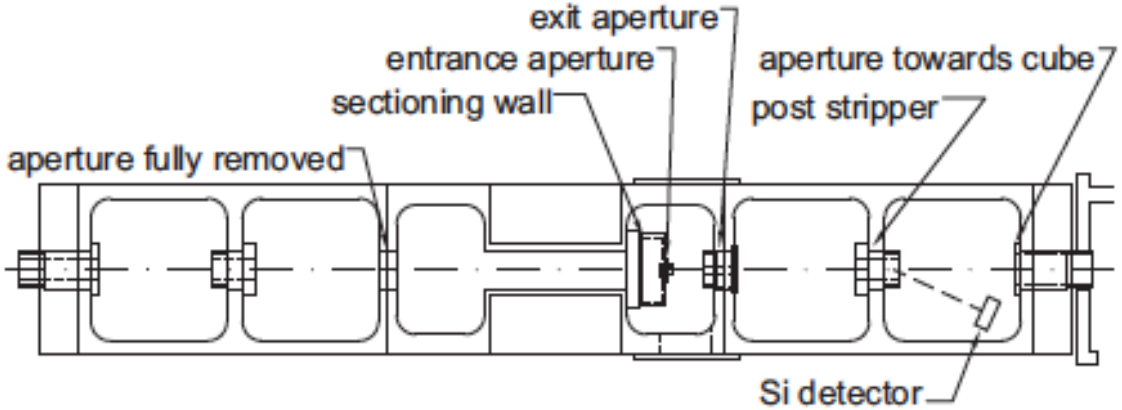

TABLE I. Measured values, results, and relevant quantities used in the target thickness determination.

Ion	E_{Lab} (MeV)	$\Delta B(^4\mathrm{He})$ (mT)	$\varepsilon(^4\mathrm{He})$ (keV cm^2/10^{18})	$\Delta E(^4\mathrm{He})$ (keV)	Thickness (10^{18}/cm^2)
^{12}C	3.5	6.13	64.3	43.3 ± 3.1	0.67 ± 0.11
^{14}N	3.0	7.72	79.0	46.7 ± 2.5	0.59 ± 0.09
^{15}N	6.3	3.39	85.0	43.3 ± 4.8	0.51 ± 0.10
^{16}O	4.5	5.05	89.8	52.6 ± 3.5	0.59 ± 0.08
^{19}F	4.8	5.09	103	50.2 ± 2.7	0.49 ± 0.06
^{19}F	3.5	5.85	94.7	49.5 ± 3.0	0.52 ± 0.07

Measurement of the energy loss of several ions, using CSSM as an analyzer. The uncertainties are due to the ΔB determination, and to uncertainty on the stopping power values. Operating the target at a He pressure of 4 mbar:

$$(0.54 \pm 0.03) \times 10^{18}\ \mathrm{atoms/cm^2}.$$

Helium Gas Target characterization

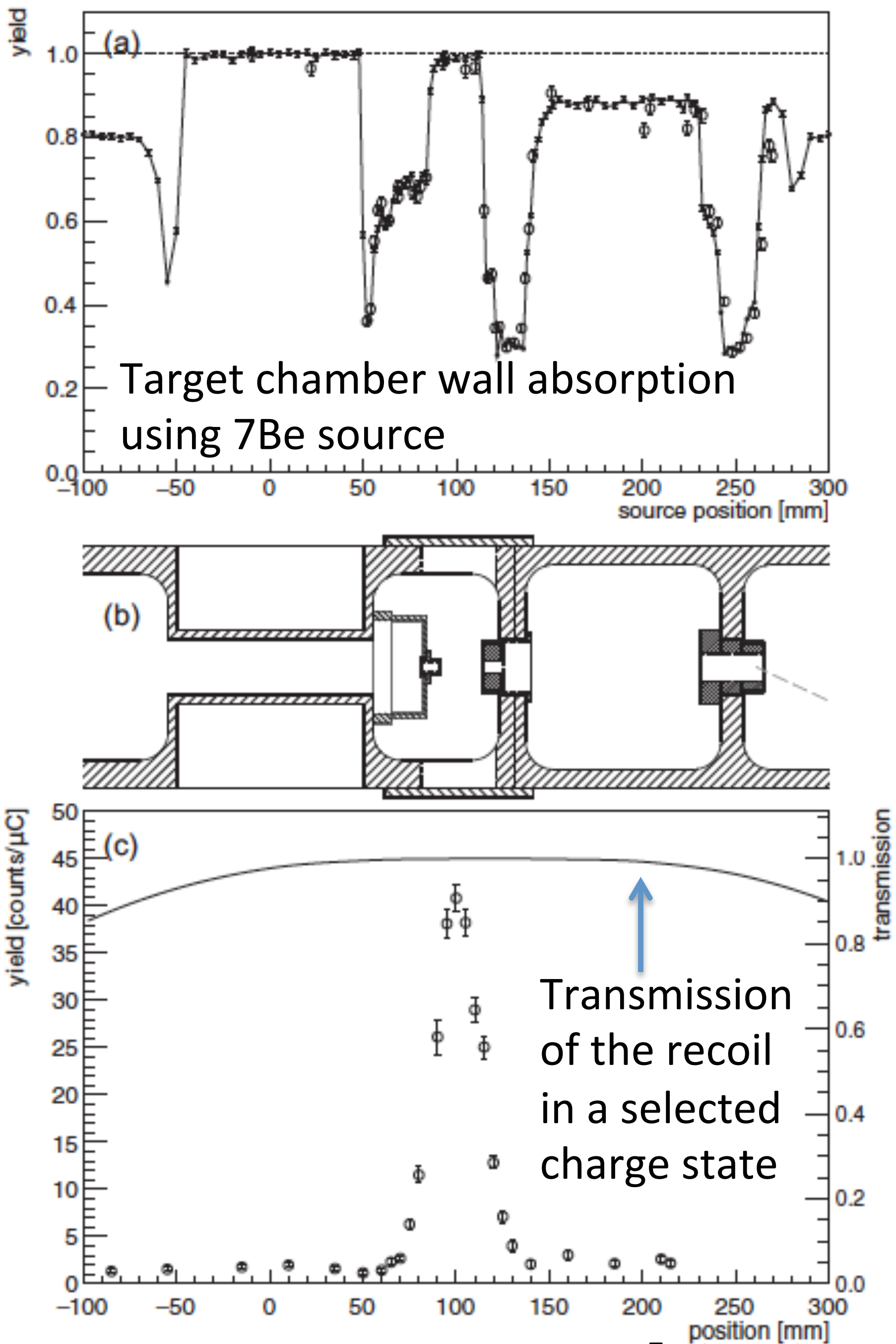

Gas density profile studied using ^{7}Li(α,α') reaction

The distribution of the He was determined measuring the yield of the broad resonance at Γ_{cm} = 130 keV in ^{7}Li(α,$\gamma\alpha'$) ^{7}Li at the energy of E_{lab} = 3325 keV.

To correct the observed yield for the absorption by chamber walls, the experimental setup was simulated with GEANT4.

The simulation was validated against a measurement of the realtive attenuation of a ^{7}Be γ-ray source, that could be moved along the beam axis of the target chamber.

Charge State probability: P of post-stripper

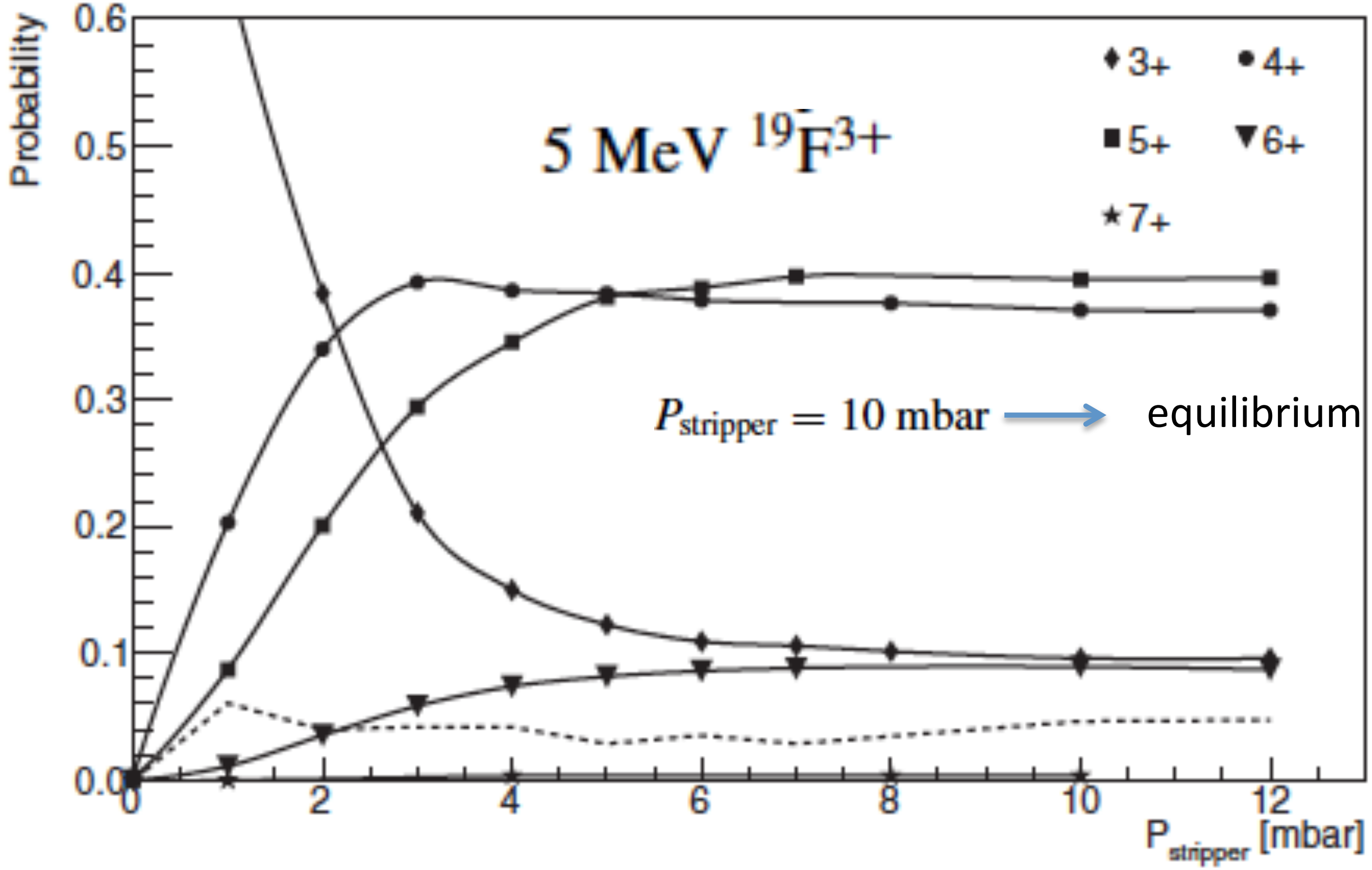

FIG. 4. Charge state probability of ^{19}F ions as a function of the Ar post-stripper inlet pressure $P_{stripper}$ at 5.0 MeV beam energy. Lines connecting the points are to guide the eye only. The dotted line represents the unmeasured current at this energy, due to nonaccessible 1+, 2+ charge states and further charge exchanging in the CSSM chamber; see text for details.

Charge State probability of ^{19}F vs E

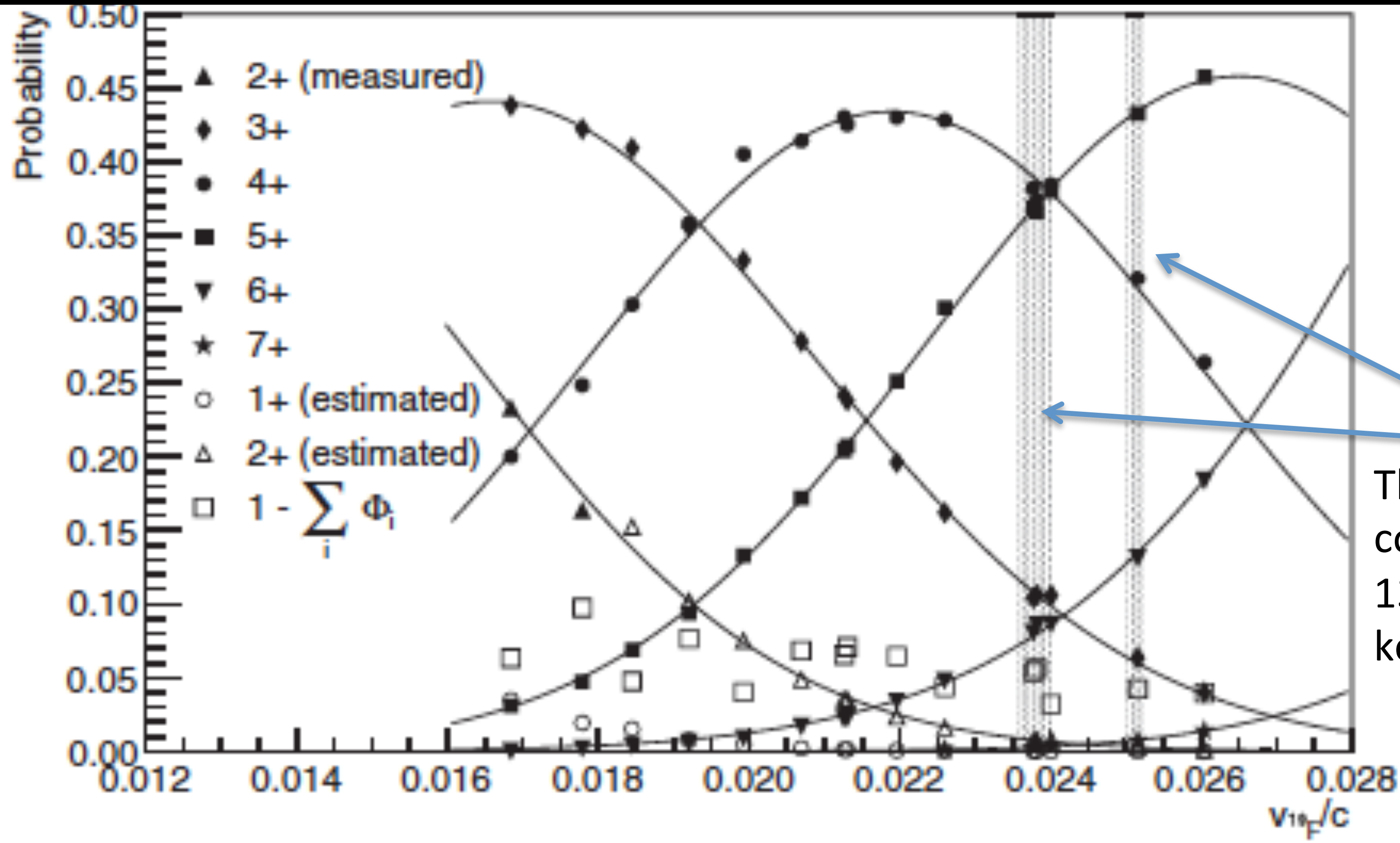

Those areas correspond to 1327 and 1487 keV resonances.

Due to the limitations of CSSM field, not all the charge states could be measured at all energies. The unmeasured charge state probabilities, namely 1+ qand 2+, were estimated considering that, at a given energy, the probability as a function of the charge state can be assumed Gaussian.

Acceptance

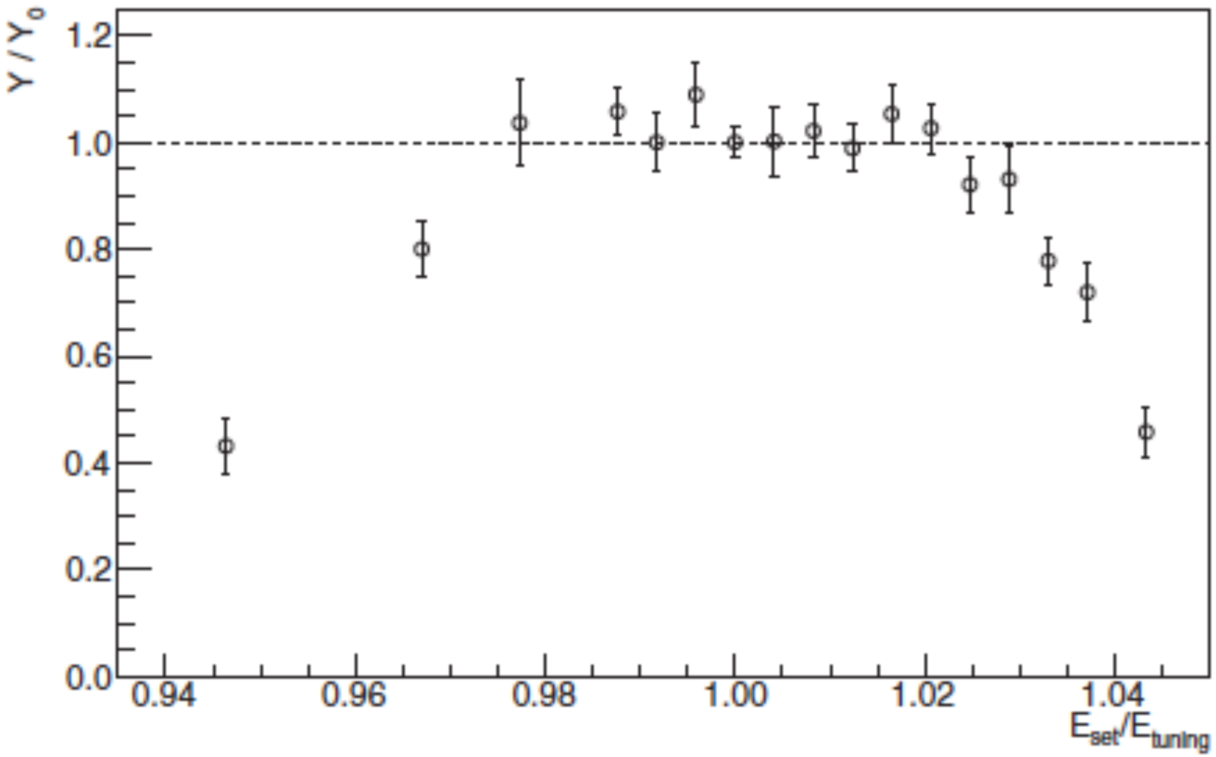

100% Transmission using ^{19}F ion beam using a electrostatic deflection unit to mimic the recoils cone.

As a further test we set the separator in the middle of the plateau of 1323 keV resonance, then we varied the energy to each the separator was tuned.

FIG. 6. Ratio of the observed yield Y with respect to the central yield Y_0 of the $E_{c.m.} = 1323$ keV resonance as a function of the energy set for the separator.

Results: particle identification

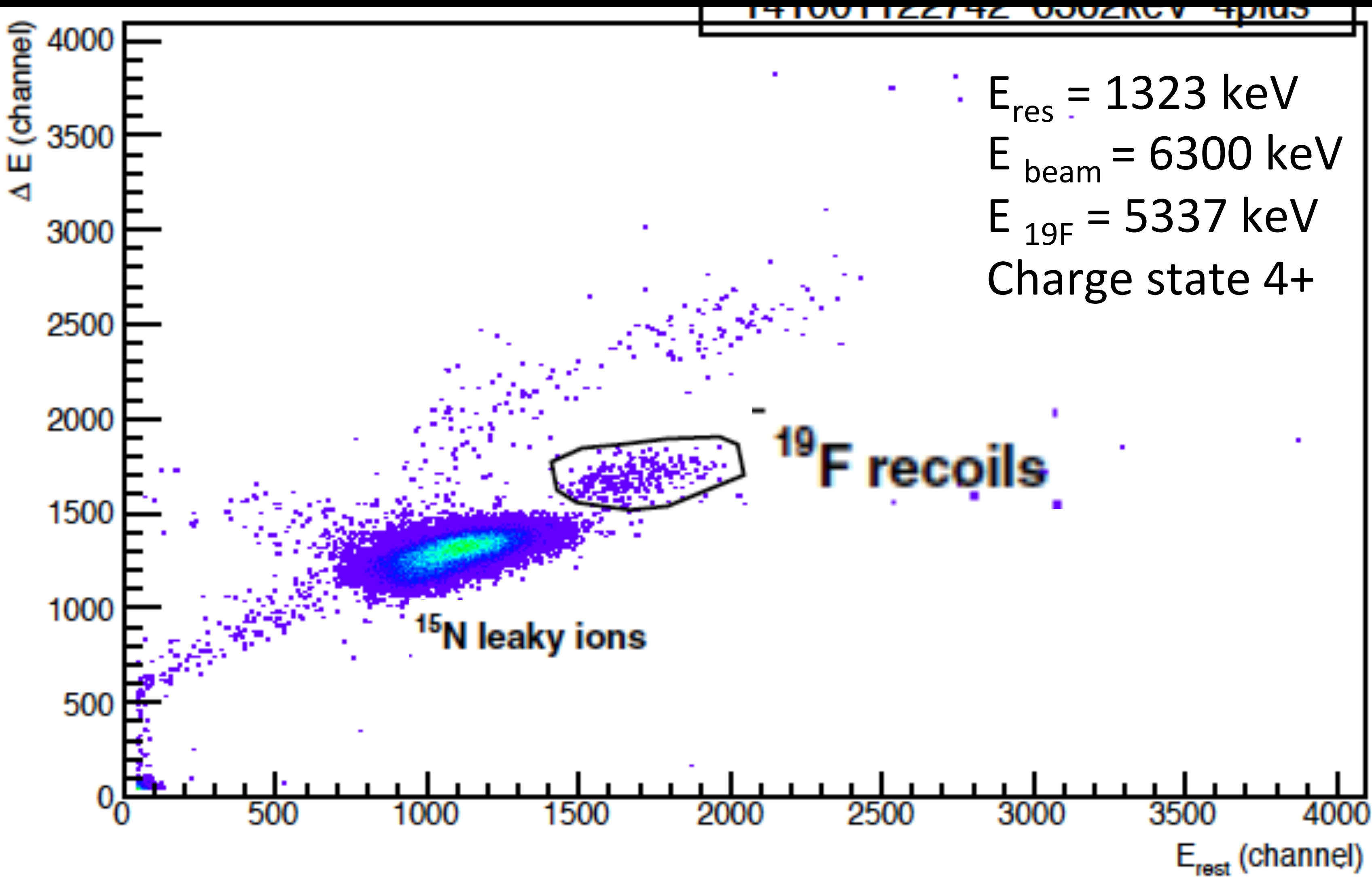

Results: particle identification

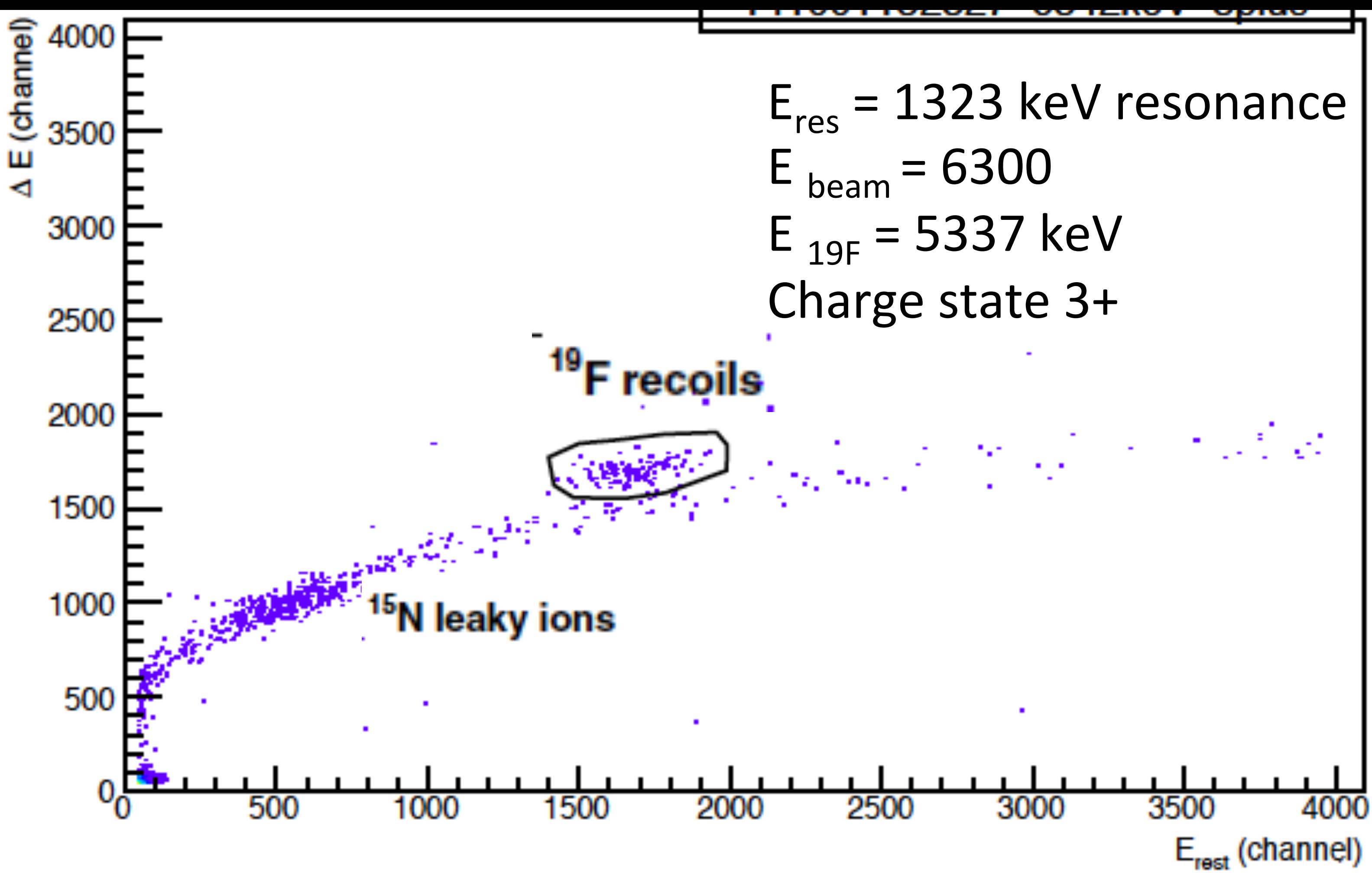

E_{res} = 1323 keV resonance
E_{beam} = 6300
E_{19F} = 5337 keV
Charge state 3+

Results: particle identification

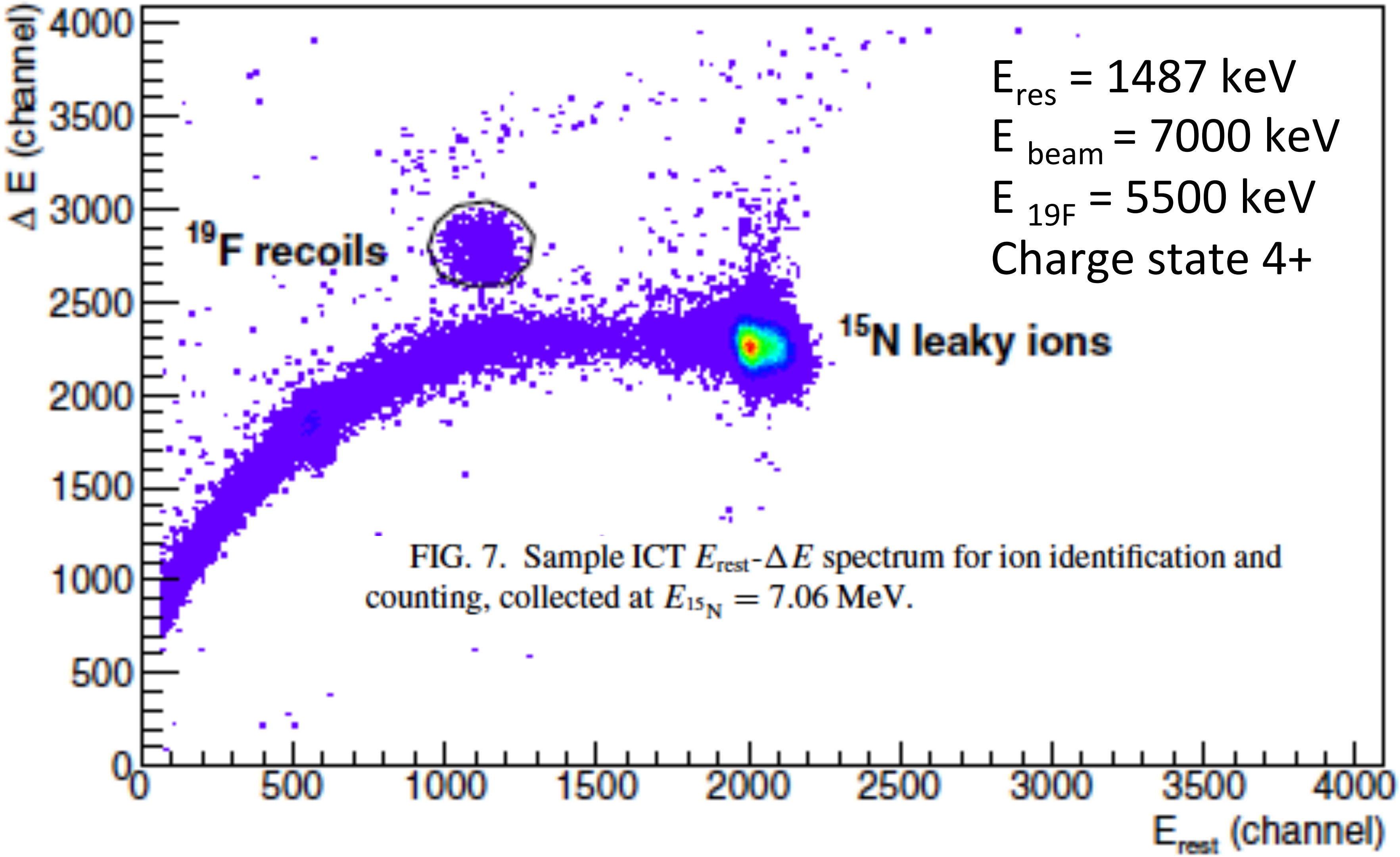

FIG. 7. Sample ICT E_{rest}-ΔE spectrum for ion identification and counting, collected at $E_{^{15}N} = 7.06$ MeV.

Results: 1323 keV resonance

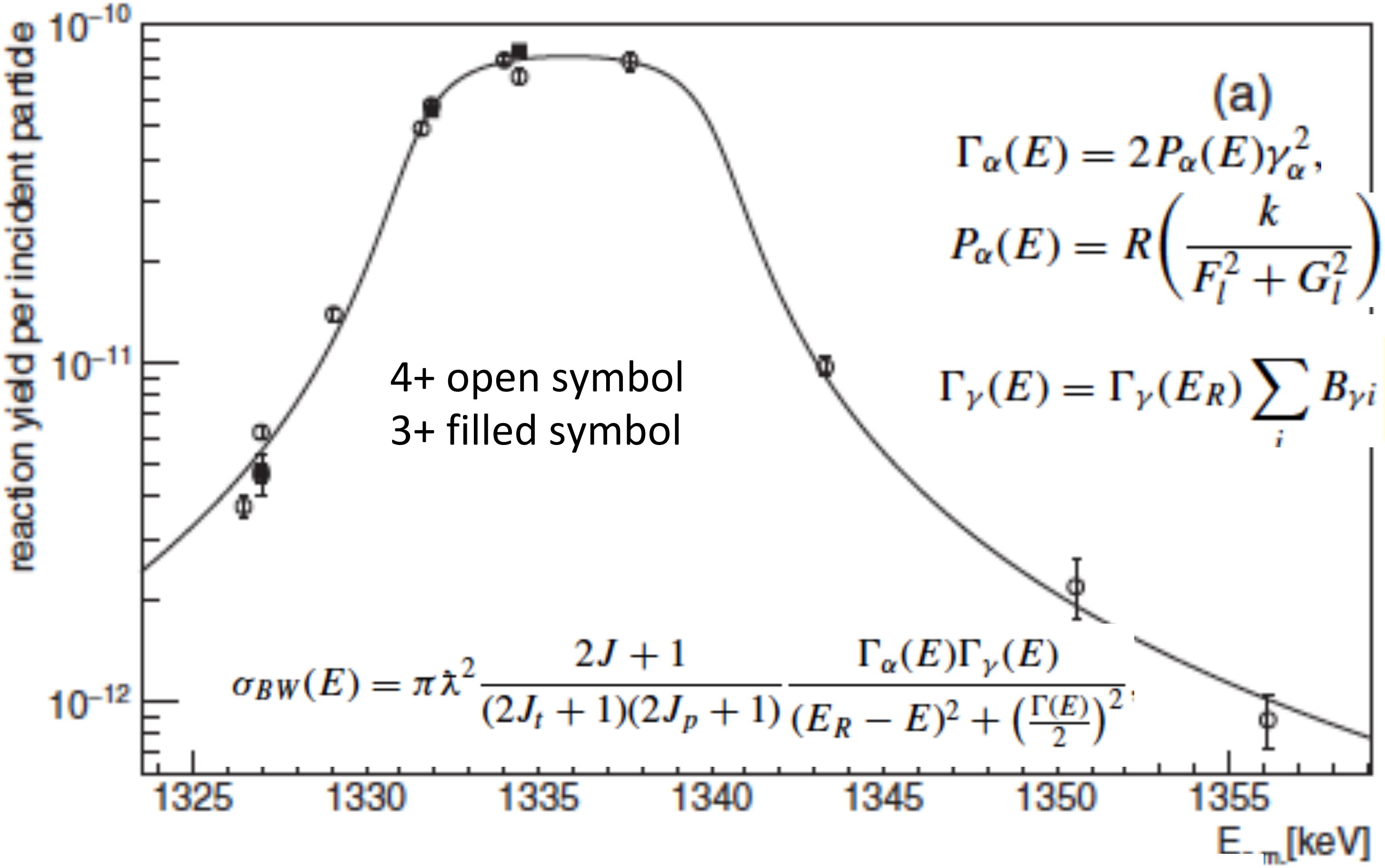

$$\Gamma_\alpha(E) = 2P_\alpha(E)\gamma_\alpha^2,$$

$$P_\alpha(E) = R\left(\frac{k}{F_l^2 + G_l^2}\right)$$

$$\Gamma_\gamma(E) = \Gamma_\gamma(E_R)\sum_i B_{\gamma i}\left[\frac{E + Q - E_{xi}}{E_R + Q - E_{xi}}\right]^{2L_i+1}$$

$$\sigma_{BW}(E) = \pi\lambda\!\!\!^{-2}\frac{2J+1}{(2J_t+1)(2J_p+1)}\frac{\Gamma_\alpha(E)\Gamma_\gamma(E)}{(E_R - E)^2 + \left(\frac{\Gamma(E)}{2}\right)^2}$$

	This work	Ref. [29]	Ref. [30]
	1323 keV resonance		
E_R (keV)	1331.4 ± 1.6	1323 ± 2	
Γ_γ (eV)	1.62 ± 0.09		1.69 ± 0.14
Γ_α (keV)	2.51 ± 0.10		1.3 ± 0.5

Results: 1487 keV resonance

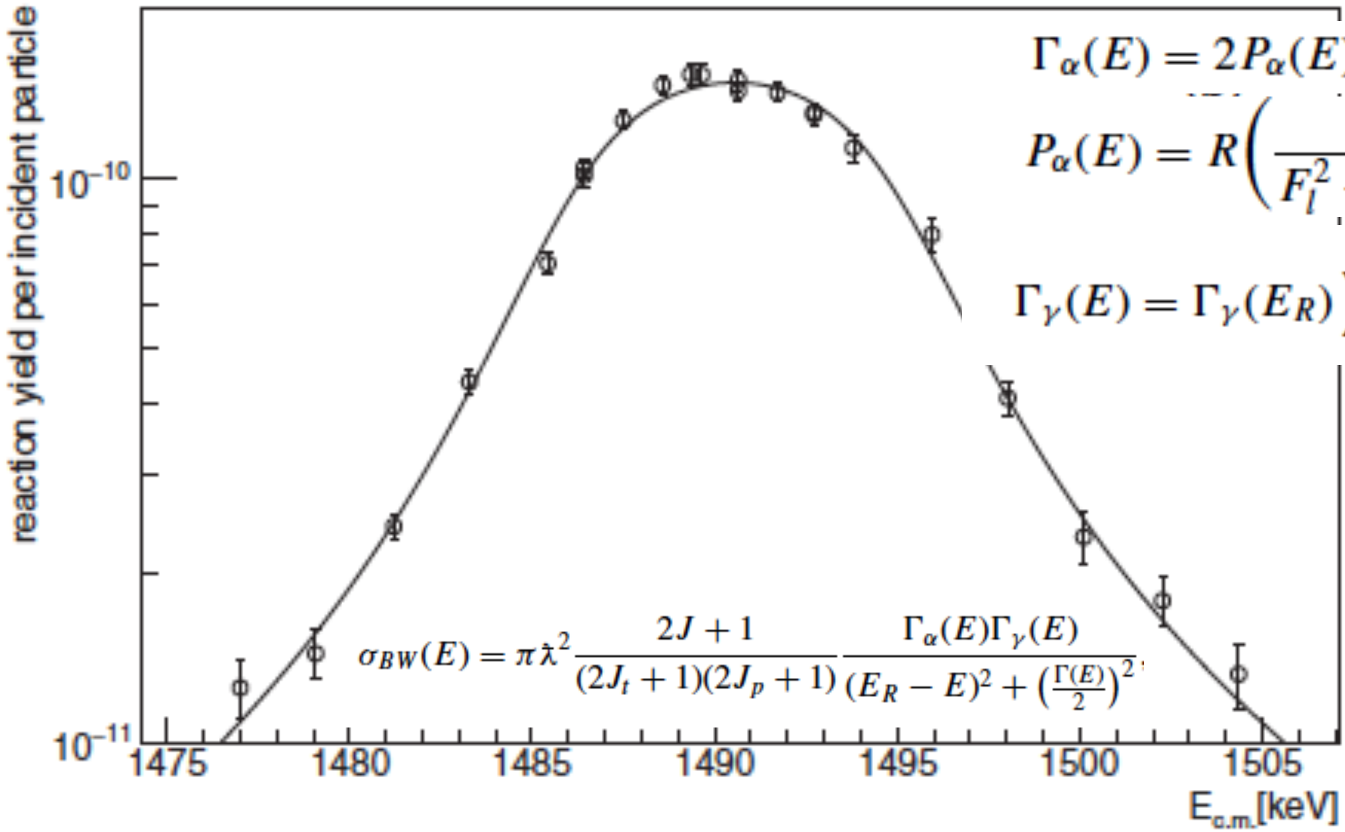

$$\sigma_{BW}(E) = \pi \lambda\!\!\!^{-2} \frac{2J+1}{(2J_t+1)(2J_p+1)} \frac{\Gamma_\alpha(E)\Gamma_\gamma(E)}{(E_R - E)^2 + \left(\frac{\Gamma(E)}{2}\right)^2}$$

$$\Gamma_\alpha(E) = 2P_\alpha(E)\gamma_\alpha^2,$$

$$P_\alpha(E) = R\left(\frac{k}{F_l^2 + G_l^2}\right)$$

$$\Gamma_\gamma(E) = \Gamma_\gamma(E_R)\sum_i B_{\gamma i}\left[\frac{E + Q - E_{xi}}{E_R + Q - E_{xi}}\right]^{2L_i+1}$$

	This work	Ref. [29]	Ref. [30]
	1487 keV resonance		
E_R (keV)	1486.1 ± 1.9	1486.7 ± 1.7	
Γ_γ (eV)	2.2 ± 0.2	2.13	1.78 ± 0.17
Γ_α (keV)	6.0 ± 0.3	4 ± 1	4.7 ± 1.6

LSF analysis

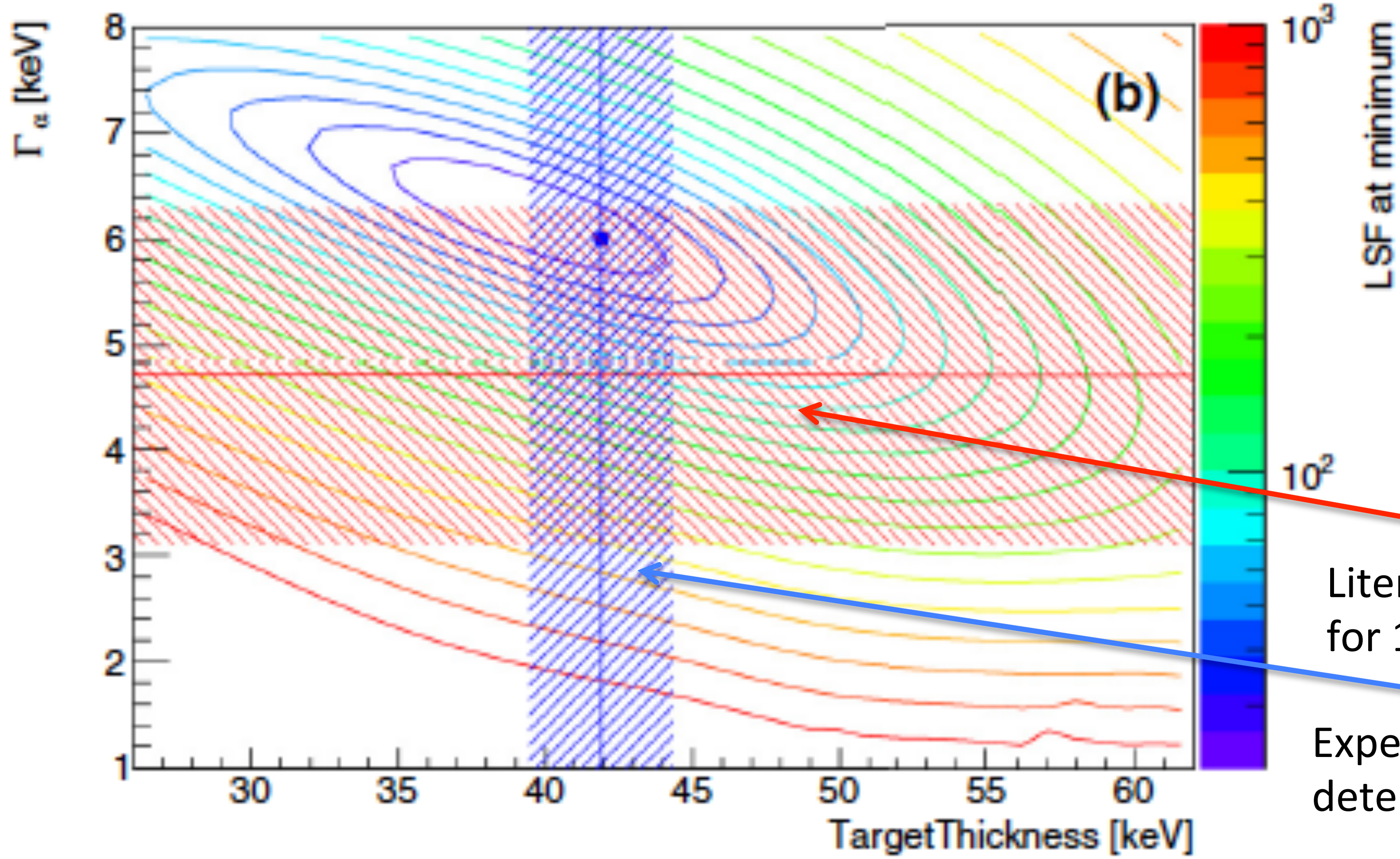

Literature value of Γ_α for 1487 keV Res.

Experimental determination of T_t

To exclude that our results of Γ_α were an artifact of a wrong target thickness determination, we choose uniformly distributed random values for T_t and Γ_α and the LSF was minimized with respect to the other parameters. For both resonances T_t leads to fit of data with LSF close to the absolute minimum excluding possible issues.

Conclusions

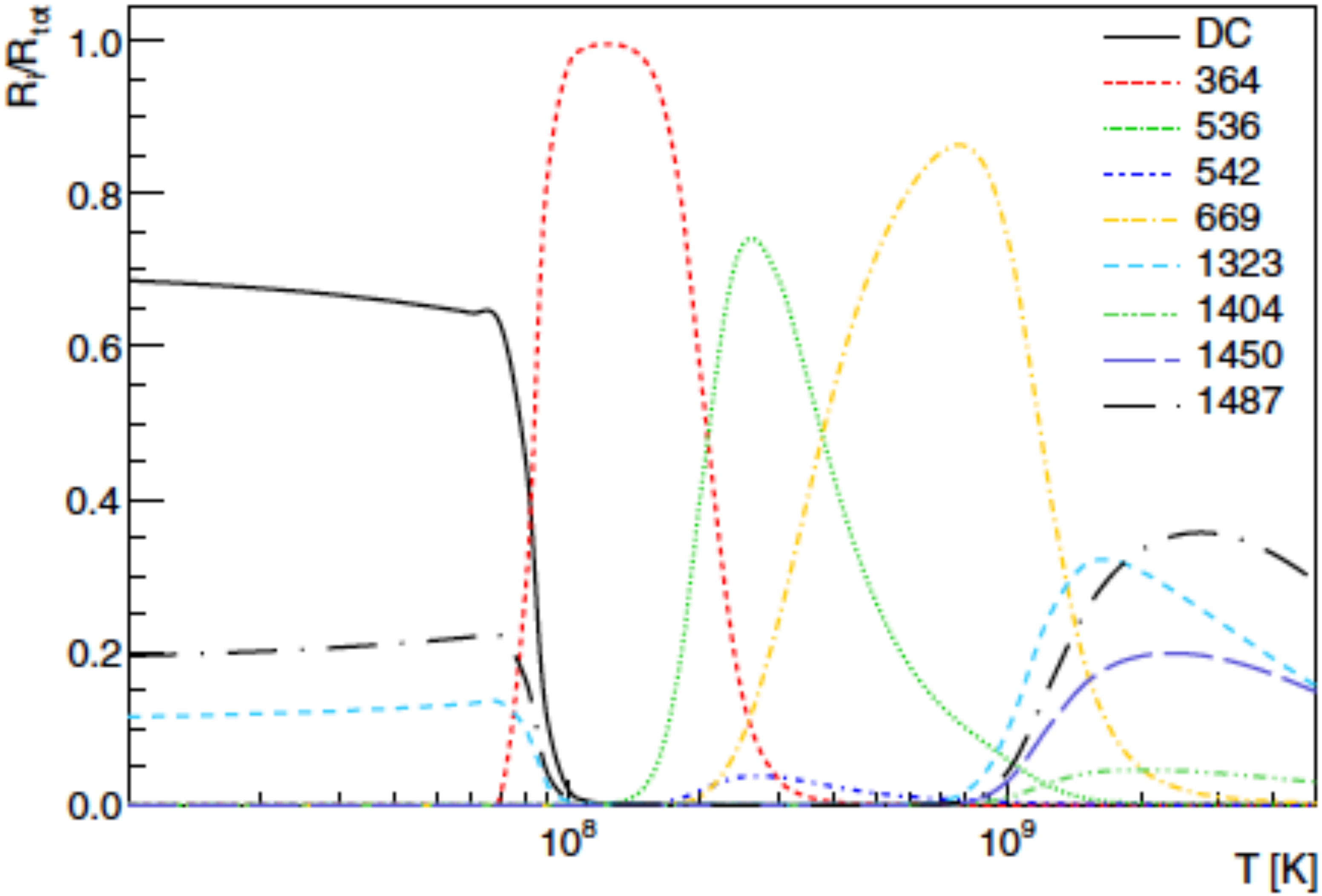

A. DI LEVA *et al.* PHYSICAL REVIEW C **95**, 045803 (2017)

Outlooks

- jet gas target;
- TOF as a final detector;
- Measurement of 365 keV resonance of $^{15}N(\alpha,\gamma)^{19}F$

15th International Symposium on NUCLEI IN THE COSMOS

24-29 June 2018

Laboratori Nazionali del Gran Sasso

Assergi, Italy

http://nic2018.lngs.infn.it

INFN
Laboratori Nazionali del Gran Sasso

GRAN SASSO SCIENCE INSTITUTE
SCHOOL OF ADVANCED STUDIES
Scuola Universitaria Superiore

Seconda Università degli Studi di Napoli
SUN